AIAA JOURNAL
Vol. 35, No. 8, August 1997

Finite Element Adaptive Method for Hypersonic Thermochemical Nonequilibrium Flows

Djaffar Ait-Ali-Yahia* and Wagdi G. Habashi†
Concordia University, Montreal, Quebec H3G 1M8, Canada

A finite element, segregated method is presented for two-dimensional hypersonic, thermochemical nonequilibrium flows, with emphasis on efficiently resolving shock waves by mesh adaptation. The governing equations are decoupled into three systems of partial differential equations (PDE), gasdynamic, chemical, and vibrational systems, and then solved in a sequential manner. This approach has the advantage of reducing reacting flow problems to a manageable computational level and offers the possibility of applying the most appropriate scheme for each system to achieve the best global convergence. Each system of PDE is integrated by an implicit time marching technique, with a Galerkin–finite element method used in space. The flow solver is coupled to an adaptive procedure based on an a posteriori error estimate and a mesh movement strategy with no orthogonality constraints. The overall methodology is validated on nitrogen and air hypersonic flows and experimental results are correctly reproduced using relatively coarse, but adapted meshes.

Introduction

INTEREST in the area of hypersonic vehicles has increased the need for advanced computational fluid dynamics codes to serve in the numerical prediction of thermochemical nonequilibrium flows. The flowfields of such problems are chemically reacting, and molecular species are vibrationally excited so numerical analyses based on an ideal gas assumption are inappropriate. At the other extreme, simulations including ionization and thermochemical nonequilibrium phenomena remain an onerous task even on today's supercomputers. Therefore, a cost-effective solution of the problem requires the proper modeling of the phenomena involved, along with an efficient solver.

An accurate prediction of such flows includes the resolution of very strong detached shocks, followed by extremely fast vibrational relaxation phenomenon and intense chemical reactions. The regions containing those important phenomena are characterized by steep directional gradients of flow variables; their limits are unknown a priori and are embedded in regions where the flow variables vary more smoothly. Hence, an accurate numerical simulation of such flows would require a fine grid, compounding the difficulty of the problem.

An efficient alternative consists of seeking numerical solutions on anisotropic adapted grids.[1,2] In the past, the use of this idea has been restricted to unstructured grids such as triangular elements. However, as shown by the present authors,[3] a large degree of grid anisotropy can also be introduced in structured grids through an improved mesh movement scheme. This approach, based on a judiciously selected a posteriori error estimate can greatly improve the quality of the solutions by relocating the nodes of an initial grid along directions with rapidly changing flow variables.

As to time discretization, most of steady-state solutions of hypersonic flows are computed by marching the unsteady governing equations in pseudotime using explicit or implicit integration techniques. The explicit approach[4–6] was very popular in the mid 1980s due to its moderate demand on computer resources. For fast reaction problems, however, the stiffness of the source terms may limit the permissible time step to very small values, resulting in large computational times.

Received Aug. 17, 1996; revision received April 30, 1997; accepted for publication April 30, 1997.

*Research Associate, Computational Fluid Dynamics Laboratory, Department of Mechanical Engineering, 1455 de Maisonneuve Blvd. W., ER 301. Member AIAA.

†Director, Computational Fluid Dynamics Laboratory, Department of Mechanical Engineering. Associate Fellow AIAA.

Bussing and Murman[7] have improved this numerical stability limitation by treating the chemical source terms in an implicit manner and the convective terms in an explicit manner. It has been shown that this has the effect of rescaling the governing equations in time such that all gasdynamic and chemical phenomena evolve at comparable pseudotime scales. This formulation leads to a point-implicit scheme where block matrices must be inverted at each point.

Among modern alternatives, the implicit methods have achieved significant success due to their robustness.[8–10] In this type of scheme, the gasdynamic, species transport, and vibrational energy equations are assembled over the domain or part of it and solved simultaneously in a coupled fashion. However, for typical hypersonic reacting problems, such a formulation results in a large system of equations that is quite demanding in terms of memory.

In the present study, this drawback is eliminated by segregating the governing equations into three systems of partial differential equations (PDE), gasdynamic, chemical, and vibrational systems, and solved in a sequential but implicit manner. This formulation, also labeled as loosely coupled approach, enjoys the robustness of an implicit formulation, while keeping memory requirements to a manageable level. It also allows each system of PDE to be integrated by the most appropriate algorithm, in an attempt to achieve the best global convergence. This particular feature makes the present approach quite attractive for applications having stiff source terms, as well as easy to retrofit into existing gasdynamic codes.

In summary, the current paper proposes an implicit, Galerkin–finite element, segregated method for hypersonic, thermochemical nonequilibrium flows, with an emphasis on resolving directional flow features, such as shocks, by an anisotropic mesh adaptation procedure. The number of chemical equations could be very high but is drastically reduced by neglecting ionization phenomena, thus leaving one to model a dissociated air by only the five neutral species: O, N, NO, O_2, and N_2.

Governing Equations

The conservation form of the mass, momentum, total internal energy, species mass fraction, and vibrational energy equations describing a thermochemical nonequilibrium flow may be written as

$$\boldsymbol{Q}_{,t} + \boldsymbol{F}_{i,i} = \boldsymbol{S} \tag{1}$$

where $\boldsymbol{Q}$ is the vector of the conservative variables, $\boldsymbol{F}_i$ is the vector of convective fluxes, and $\boldsymbol{S}$ is the vector of sources. For a gas mixture with the five species O, N, NO, O_2, and N_2 that will be identified by the subscripts 1–5, the components of vectors $\boldsymbol{Q}$, $\boldsymbol{F}_i$, and $\boldsymbol{S}$, in two-dimensional problems are

$$\boldsymbol{Q} = \begin{bmatrix} \rho \\ \rho v_1 \\ \rho v_2 \\ \rho e \\ \rho c_1 \\ \vdots \\ \rho c_4 \\ \rho c_3 e_{v3} \\ \vdots \\ \rho c_5 e_{v5} \end{bmatrix}, \qquad \boldsymbol{F}_i = \begin{bmatrix} \rho v_i \\ \rho v_1 v_i + p\delta_{1i} \\ \rho v_2 v_i + p\delta_{2i} \\ (\rho e + p) v_i \\ \rho c_1 v_i \\ \vdots \\ \rho c_4 v_i \\ \rho c_3 e_{v3} v_i \\ \vdots \\ \rho c_5 e_{v5} v_i \end{bmatrix}$$

$$\boldsymbol{S} = \begin{bmatrix} 0 \\ 0 \\ 0 \\ 0 \\ S_1^c \\ \vdots \\ S_4^c \\ q_{T\_v3} + q_{v\_v3} + S_3^c e_{v3} \\ \vdots \\ q_{T\_v5} + q_{v\_v5} + S_5^c e_{v5} \end{bmatrix} \tag{2}$$

where ρ is the mixture density, v_i the velocity components, p the pressure of the mixture, c_s the mass fraction of the species s, e the specific total internal energy, and e_{vs} the vibrational energy of the molecular species s. Here, S_s^c denotes the rate of production of the chemical species s and q_{T_vs} and q_{v_vs} are, respectively, the rates of translation–vibration and vibration–vibration energy exchange. In addition, the global mass conservation condition dictates that

$$\sum_{s=1}^{N_s} c_s = 1 \tag{3}$$

where N_s represents the total number of chemical species, i.e., five.

The number of species transport equations may be further reduced, in the case of inviscid flows, by replacing any one of them by the algebraic equation for conservation of elemental nitrogen to oxygen ratio in air. Assuming the molar concentration of oxygen and nitrogen in air to be 21 and 79%, respectively, the elemental conservation condition reads

$$\frac{c_1/\mathcal{M} + c_3/\mathcal{M} + 2c_4/\mathcal{M}}{c_2/\mathcal{M} + c_3/\mathcal{M} + 2c_5/\mathcal{M}} = \frac{21}{79} \tag{4}$$

where $\mathcal{M}$ is the molecular weight of species s.

Vibrational Model

We assume that translational and rotational modes are in equilibrium and, hence, can be characterized by a single temperature T. Furthermore, the two-temperature model is adopted, meaning that all molecular species are characterized by the same vibrational temperature T_v. This model requires the solution of a single conservation equation for the total vibrational energy defined by

$$e_v = \sum_{s=1}^{N_s} c_s e_{vs} = \sum_{s=1}^{N_s} \frac{c_s \mathcal{R} \theta_{vs}}{\exp(\theta_{vs}/T_v) - 1} \tag{5}$$

where θ_{vs} refer to the vibrational characteristic temperatures and are provided in Table 1. The set of vibrational energy equations of the system (1), thus, are replaced by a single vibrational energy equation, resulting from their summation.

The translation–vibration energy exchange rate is principally modeled by the Landau–Teller equation,[11] which is extended to gas mixtures as

$$q_{T\_vs} = \rho c_s \frac{e_{vs}^*(T) - e_{vs}(T_v)}{\langle \tau_s^{L-T} \rangle} \tag{6}$$

Table 1 Characteristic vibrational temperatures and heats of formation

Species	O	N	NO	O_2	N_2
θ_{vs}	——	——	2817	2239	3395
h_s^o	1.543119×10^7	3.362161×10^7	2.996123×10^6	0	0

where $e_{vs}^*(T)$ is the vibrational energy the species s would have if it was in equilibrium at the translational temperature T. Here $\langle \tau_s^{L-T} \rangle$ represents the molar-averaged Landau–Teller relaxation time and is given by Lee[12] as

$$\langle \tau_s^{L-T} \rangle = \frac{\sum_{l=1}^{N_s} \chi_l}{\sum_{l=1}^{N_s} \chi_l / \tau_{sl}^{L-T}} \tag{7}$$

where the Landau–Teller interspecies relaxation time τ_{sl}^{L-T} is correlated by Millikan and White's[13] semiempirical formula as follows:

$$\tau_{sl}^{L-T} = (1/p) \exp\left[\mathcal{A} \left(T^{-\frac{1}{3}} - 0.015 \mu_{sl}^{\frac{1}{4}} \right) - 18.42 \right]$$

$$\mathcal{A} = 1.16 \times 10^{-3} \mu_{sl}^{\frac{1}{2}} \theta_{vs}^{\frac{4}{3}}$$

$$\mu_{sl} = \frac{\mathcal{M}_s \mathcal{M}_l}{\mathcal{M}_s + \mathcal{M}_l}$$

For temperatures higher than 8000 K, the Millikan and White[13] formula, however, results in unrealistically small relaxation times, due to an overprediction of the collision cross section. To correct this inadequacy, Park[14] suggested adding a new relaxation time τ_s^P to the molar-averaged previous Landau–Teller relaxation time, that is,

$$\tau_s^P = (\xi_s \sigma_v X_s)^{-1} \tag{8}$$

where $\xi_s = \sqrt{8RT/\pi \mathcal{M}_s}$ represents the average molecular speed of species s and X_s the number density of colliding particles. The limiting collision cross section σ_v is approximated by the expression originally developed for nitrogen: $\sigma_v = 10^{-21}(50{,}000/T)^2$.

Chemical Model

At high temperatures, chemical reactions occur in gas flows resulting in changes in the amount of mass of each chemical species. This mass transfer process is controlled by the rate of production S_s^c that may be expressed for the species s as

$$S_s^c = \mathcal{M}_s \sum_{r=1}^{N_r} (\nu''_{sr} - \nu'_{sr})(R_{\text{fr}} - R_{\text{br}}) \tag{9}$$

where r refers to the reaction index, N_r is the total number of reactions, and ν'_{sr} and ν''_{sr} are the stoichiometric coefficients for the reactants and the products, respectively. The forward rate R_{fr} and the backward rate R_{br} are given by

$$R_{\text{fr}} = k_{\text{fr}}(T) \prod_{s=1}^{N_s} \left(\frac{\rho c_l}{\mathcal{M}_l} \right)^{\nu'_{lr}}, \qquad R_{\text{br}} = k_{\text{br}}(T) \prod_{s=1}^{N_s} \left(\frac{\rho c_l}{\mathcal{M}_l} \right)^{\nu''_{lr}} \tag{10}$$

Here, k_{fr} and k_{br} are the forward and the backward reaction rate coefficients for the reaction r and possess the following Arrhenius form:

$$k_{\text{fr}}(T) = C_{\text{fr}} T^{\eta_{\text{fr}}} \exp\left(-\frac{\theta_{d,\text{fr}}}{T} \right)$$

$$k_{\text{br}}(T) = \frac{k_{\text{fr}}(T)}{k_{eqr}(T)} \tag{11}$$

where the rate constants C_{fr}, η_{fr} and $\theta_{d,\text{fr}}$ are given by Park's reaction model.[15] This model includes 15 dissociation and 2 shuffle reactions among the five neutral species.

Vibration–dissociation coupling is introduced through a rate controlling temperature $T_a = \sqrt{T T_v}$, which replaces the translational temperature in the computation of species rate of production, as proposed by Park.[14]

Numerical Scheme

After the modeling simplifications are introduced into the governing Eqs. (1), the resulting system is decoupled into three systems of PDE.

Gasdynamic system:

$$\boldsymbol{Q}^g_{,t} + \boldsymbol{F}^g_{i,i} = 0$$

$$\boldsymbol{Q}^g = \begin{bmatrix} \rho \\ \rho v_1 \\ \rho v_2 \\ \rho e \end{bmatrix}, \qquad \boldsymbol{F}^g_i = \begin{bmatrix} \rho v_i \\ \rho v_1 v_i + p\delta_{1i} \\ \rho v_2 v_i + p\delta_{2i} \\ (\rho e + p) v_i \end{bmatrix} \tag{12}$$

Chemical system:

$$\boldsymbol{Q}^c_{,t} + \boldsymbol{F}^c_{i,i} = \boldsymbol{S}^c$$

$$\boldsymbol{Q}^c = \begin{bmatrix} \rho c_1 \\ \rho c_2 \\ \rho c_3 \end{bmatrix}, \qquad \boldsymbol{F}^c_i = \begin{bmatrix} \rho c_1 v_i \\ \rho c_2 v_i \\ \rho c_3 v_i \end{bmatrix}, \qquad \boldsymbol{S}^c = \begin{bmatrix} S^c_1 \\ S^c_2 \\ S^c_3 \end{bmatrix} \tag{13}$$

Vibrational system:

$$\boldsymbol{Q}^v_{,t} + \boldsymbol{F}^v_{i,i} = \boldsymbol{S}^v$$

$$\boldsymbol{Q}^v = [\rho e_v], \qquad \boldsymbol{F}^v_i = [\rho e_v v_i]$$

$$\boldsymbol{S}^v = \left[\sum_{s=1}^{N_s} q_{T-vs} + \sum_{s=1}^{N_s} S^c_s e_{vs} \right] \tag{14}$$

The present numerical method is described in more detail in Ref. 16. The thermochemical nonequilibrium effects are introduced into the gasdynamic code,[3] initially developed for calorically ideal gases, by replacing the standard ratio of specific heats γ by an equivalent $\tilde{\gamma}$ into the flux Jacobian matrices. Such an approach, introduced by Gnoffo,[17] is highly suitable for existing gasdynamic solvers and leads to flexible codes that are capable of handling a large variety of compressible flow problems, ranging from subsonic to hypersonic speeds, in a cost-effective manner.

In summary, the equation of state of the real gas is cast into the form of an ideal gas

$$p = (\tilde{\gamma} - 1)\rho\varepsilon \tag{15}$$

permitting the reuse of the gasdynamic Jacobian matrices that were developed for calorically perfect gases. The variable ε denotes the internal energy, and $\tilde{\gamma}$ is a function that remains between 1 and $\frac{5}{3}$, even when the values of other thermodynamic variables vary over several orders of magnitude.[18] The value of $\tilde{\gamma}$ is deduced from Eq. (15) as

$$\tilde{\gamma} = 1 + (p/\rho\varepsilon) \tag{16}$$

in such a way that the value of the pressure matches the one given by the real gas. In thermochemical equilibrium situations, the pressure is usually determined from an equilibrium curve fit $p = p(\rho, \varepsilon)$ and then the equivalent $\tilde{\gamma}$ is evaluated according to Eq. (16).

The present finite element method limits the influence of the equivalent $\tilde{\gamma}$ to the left-hand side of the resulting discrete system, which is viewed as a preconditioning matrix and, consequently, has no influence on the steady-state solution, as far as accuracy is concerned.

To prevent unrealistic species mass fractions, i.e., $c_s \notin [0, 1]$, that may result in the first Newton iterations, the chemical source terms are relaxed according to the following formula:

$$\tilde{S}^c_s = \frac{S^c_s - |S^c_s|}{2\max(\epsilon, c_s)} c_s + \frac{S^c_s + |S^c_s|}{2\max(\epsilon, 1 - c_s)}(1 - c_s) \tag{17}$$

where ϵ refers to a small constant of order of 10^{-10}.

For an endothermic reaction ($S^c_s > 0$), the first term on the right-hand side (RHS) of Eq. (17) vanishes and the source term expression becomes

$$\tilde{S}^c_s = \begin{cases} S^c_s & \text{if} \quad c_s \le (1 - \epsilon) \\ S^c_s (1 - c_s)/\epsilon & \text{otherwise} \end{cases} \tag{18}$$

Therefore, the source term is only corrected by a factor of $(1 - c_s)/\epsilon$ in the case when the product concentration c_s approaches unity, i.e., $c_s > (1 - \epsilon)$.

For an exothermic reaction ($S^c_s < 0$), the second term on the RHS of Eq. (17) vanishes and the source term may be rewritten as

$$\tilde{S}^c_s = \begin{cases} S^c_s & \text{if} \quad c_s \ge \epsilon \\ S^c_s c_s/\epsilon & \text{otherwise} \end{cases} \tag{19}$$

In this case, the source term is only corrected by a factor of c_s/ϵ when the reactant concentration c_s approaches zero, i.e., $c_s < \epsilon$.

Solution Procedure

The primitive variable vector $\boldsymbol{U}^g = [\rho, v_1, v_2, e]$ is first advanced in time by solving the gasdynamic system (12), and then the chemical system (13) is solved for the species mass fraction vector $\boldsymbol{U}^c = [c_1, c_2, c_3]$, using the updated velocity field and density solutions. The remaining mass fractions, c_4 and c_5, are deduced from the two algebraic equations (3) and (4) that can be rewritten as

$$c_4 = \tfrac{24}{103} - c_1 - \tfrac{8}{15}c_3, \qquad c_5 = \tfrac{79}{103} - c_2 - \tfrac{7}{15}c_3 \tag{20}$$

The total vibrational energy $\boldsymbol{U}^v = [e_v]$ is calculated by integrating the vibrational system (14), and then the vibrational temperature T_v is computed from the vibrational energy solution (5) by a Newton method. This procedure is applied for all grid nodes and at every Newton iteration and, therefore, may be computationally expensive.

Because the three neutral molecules (NO, O_2, and N_2) in air have close values of vibrational characteristic temperatures (see Table 1), a good initial estimate of the vibrational temperature could be obtained by assuming that all these molecules have the same average vibrational characteristic temperature, $\bar{\theta}_v$, defined by

$$\bar{\theta}_v = \frac{\sum_{s=3}^{N_s} c_s \theta_{vs}}{\sum_{s=3}^{N_s} c_s} \tag{21}$$

An initial estimate T^0_v can then be computed by substituting the value of $\bar{\theta}_v$ in Eq. (5), yielding

$$T^0_v = \frac{\bar{\theta}_v}{\ell n\left[1 + (\bar{\theta}_v/e_v)\sum_{s=3}^{N_s} c_s R_s\right]} \tag{22}$$

This iterative method is very efficient and usually does not need more than two Newton iterations per node to converge toward the final solution.

The translational–rotational temperature T is deduced from the following energy expression:

$$e = \sum_{s=1}^{N_s} c_s c_{vs} T + \sum_{s=1}^{N_s} c_s h^o_s + e_v + \frac{1}{2} v_i v_i \tag{23}$$

where h^o_s denote enthalpy of formations of species and are given by Table 1. Finally, if we assume each individual species behaves as a perfect gas, the pressure of the mixture may be calculated according to Dalton's law.

The computation of chemical nonequilibrium flows (with thermal equilibrium, $T = T_v$) can be easily carried out by only eliminating the vibrational system (14) from the flow solver loop. In fact, the segregated approach permits the recovery of the thermal equilibrium flows without solving additional equations and modifying the vibrational relaxation times, as is usually done in the coupled approach. In contrast with the thermal nonequilibrium solution procedure, the translational temperature is computed by a Newton method from Eq. (23).

Anisotropic Mesh Adaptation

The efficiency and accuracy of the preceding flow solver may be significantly enhanced by coupling it to a mesh adaptation procedure[3] that relies on a directional error estimate and a mesh movement scheme that is vastly improved by removing the usual constraints on grid orthogonality.[19] These two ingredients are essential for achieving grid anisotropy, and they are presented in the following sections.

Error Estimate

Consider a one-dimensional problem in which the solution u is approximated by u_h with piecewise linear interpolation. The root mean square (rms) interpolation error over an element spanning the interval $[0, h_e]$ may be defined as

$$E_e^{\text{rms}} = \frac{1}{\sqrt{120}} h_e^2 \left| \frac{\mathrm{d}^2 u_h}{\mathrm{d}x^2} \right|_e \tag{24}$$

(Ref. 3), provided that the approximate solution is exact at the nodes. The optimal mesh is thus defined as the mesh in which the rms error is equidistributed over the elements, that is,

$$h_e^2 \left| \frac{\mathrm{d}^2 u_h}{\mathrm{d}x^2} \right|_e = C \tag{25}$$

where C denotes a user-specified tolerance.

Extending this adaptation criterion to two-dimensional cases, the second derivative of u_h is now taken with respect to a given unit vector $\boldsymbol{V}$ as follows:

$$\frac{\partial^2 u_h}{\partial \boldsymbol{V}^2} = \boldsymbol{V}^T \boldsymbol{H} \boldsymbol{V} \tag{26}$$

where $\boldsymbol{H}$ represents the Hessian matrix of u_h. Because u_h is linear for each element, the second derivatives vanish. A weak formulation, however, combined with mass lumping, is applied to recover a continuous estimate of the second derivatives.

This Hessian matrix may be diagonalized as

$$\boldsymbol{H} = \boldsymbol{R}(\alpha)\, \Lambda\, \boldsymbol{R}^T(\alpha) \tag{27}$$

where Λ is the diagonal matrix of the eigenvalues of $\boldsymbol{H}$ and $\boldsymbol{R}$ is the matrix of the eigenvectors. The transformation $|\Lambda|$ is a scaling in the axes directions, and $\boldsymbol{R}$ is a rotation through an angle α that the eigenvector corresponding to the smallest eigenvalue λ_1 makes with the x_1 axis.

The u_h second derivative in any direction $\boldsymbol{V}$ is bounded by

$$\left| \frac{\partial^2 u_h}{\partial \boldsymbol{V}^2} \right| = \left| \boldsymbol{V}^T \boldsymbol{H} \boldsymbol{V} \right| \leq \boldsymbol{V}^T \bar{\boldsymbol{H}} \boldsymbol{V} \tag{28}$$

where the modified Hessian $\bar{\boldsymbol{H}}$ is defined as $\bar{\boldsymbol{H}} = \boldsymbol{R}|\Lambda|\boldsymbol{R}^T$. Hence, the one-dimensional adaptation criterion may be rewritten for two-dimensional problems as

$$h^2\, \boldsymbol{V}^T \bar{\boldsymbol{H}} \boldsymbol{V} = C \tag{29}$$

In the Peraire et al. approach,[1] $h = h_k$, with $k = 1, 2$, are two local spacings and $\boldsymbol{V} = \boldsymbol{V}_k$ are the two unit eigenvectors of the $\boldsymbol{H}$ matrix. Accordingly, the mesh criterion (29) simplifies to

$$h_k^2 |\lambda_k| = C \tag{30}$$

This equation serves to compute two local node spacings, $h_k = \sqrt{(C/|\lambda_k|)}$, in two orthogonal directions, at any point in the domain. Then, a new adapted grid is regenerated based on these local node spacings, a local stretching coefficient $\beta = (|\lambda_1|/|\lambda_2|)^{1/2}$ and the principal directions of $\bar{\boldsymbol{H}}$.

In the current approach, the error is equidistributed over the mesh edges, where $h = \|\boldsymbol{x}_J - \boldsymbol{x}_I\|$ represents the Euclidean length of an element edge $[\boldsymbol{x}_I, \boldsymbol{x}_J]$ and $\boldsymbol{V} = (\boldsymbol{x}_J - \boldsymbol{x}_I)/h$ is the unit vector that supports this edge. Thus, an optimal mesh is defined as the one in which the length of all edges, in the defined metric $\boldsymbol{H}$, is equal to $\sqrt{C}$. Because $\boldsymbol{H}$ is a function of the space coordinates, the term $\boldsymbol{V}^T \bar{\boldsymbol{H}} \boldsymbol{V}$ in Eq. (29) defines a Riemannian metric. Thus, the edge-based error estimate is computed by numerically evaluating the following formula on each edge of the grid:

$$\mathrm{d}(\boldsymbol{x}_I, \boldsymbol{x}_J) = \int_0^1 \sqrt{(\boldsymbol{x}_I - \boldsymbol{x}_J)^T \bar{\boldsymbol{H}}(l)\, (\boldsymbol{x}_I - \boldsymbol{x}_J)}\, \mathrm{d}l \tag{31}$$

Mesh Movement Scheme

In this scheme, the mesh is viewed as a network of springs whose stiffness constants are equivalent to a local measure of the error. The optimal position of the grid vertices may then be interpreted as the solution of the equations describing the equilibrium state of a spring network. This yields, for each vertex I,

$$\sum_J (\boldsymbol{x}_I - \boldsymbol{x}_J)\, k_{IJ} = 0 \tag{32}$$

where k_{IJ} denote the stiffness constants of the four springs sharing a node I and are given by

$$k_{IJ} = \frac{\mathrm{d}(\boldsymbol{x}_I, \boldsymbol{x}_J)}{\|\boldsymbol{x}_I - \boldsymbol{x}_J\|} \tag{33}$$

By lagging $\boldsymbol{x}_J$ and k_{IJ} at the previous iteration m and applying a Gauss–Seidel scheme, the position of vertex I is updated according to the expression

$$\boldsymbol{x}_I^{m+1} = \boldsymbol{x}_I^m + \omega \left[\frac{\sum_J (\boldsymbol{x}_J^* - \boldsymbol{x}_I^m)\, k_{IJ}^*}{\sum_J k_{IJ}^*} \right] \tag{34}$$

where ω is a relaxation factor and the superscript * denotes the latest value.

Numerical Results

Both flow solver and grid adaptation procedures are placed in an iterative loop, which is repeated until the lowest value of a user-specified artificial dissipation coefficient is reached. In the following, each full iteration of this loop will be called an adaptive cycle or level. For all of the test cases investigated, the temperature is the flow variable used for the error estimate.

Hypersonic Nitrogen Flow over a Cylinder

The present numerical approach is first validated on a Mach 6 partially dissociated nitrogen flow over a half-cylinder with 1-in. radius. This flow problem has been investigated experimentally by Hornung[20] and numerically by numerous authors.[8,10,21] The free-stream monatomic nitrogen mass fraction, temperature, density, and velocity are 0.073, 1833 K, 5.349×10^{-3} kg/m^3, and 5.590 km/s, respectively. The numerical simulation is performed using a five-species model by setting the mass fraction of oxygen to be 10^{-10}.

The thermochemical nonequilibrium (TCNE) calculation is initiated on a coarse grid (Fig. 1a), with 33×53 nodes distributed uniformly in both directions. The adapted grid (Fig. 1b) required five cycles of adaptation, and the corresponding solution (Fig. 1c) demonstrates the benefits of the grid adaptation in resolving a detached bow shock.

Figure 2 shows the enhancement of the predicted Mach number distribution along the stagnation line with grid adaptation cycles. In fact, the use of an appropriate grid allows a reduction of the artificial dissipation coefficient by a factor of five.

Additional calculations are performed under two different assumptions: frozen perfect gas (FPG) and chemical nonequilibrium (CNE) of a mixture of perfect gases. All of these calculations are made using the initial uniform grid that is shown in Fig. 1a, and the resulting temperature profiles along the stagnation line are compared in Fig. 3 to the TCNE case and the experimental shock position. The FPG flow assumption overestimates the standoff distance by 85%, whereas the CNE or the TCNE assumption permits a much better prediction of this distance. In addition, the CNE model produces the shortest standoff distance whereas the TCNE case gives the largest peak of the translational temperature profiles ($\approx$12,000 K) if one eliminates the FPG case, which yields unrealistically high temperatures in the shock layer.

The plot of the mass fractions of monatomic and diatomic nitrogen along the stagnation line in Fig. 4 shows that the flowfield is dominated by a high degree of reaction. It may be observed that 30% of the present diatomic nitrogen is dissociated, despite the fact that the corresponding reactions have a large activation energy.

In all of these cases, a subsonic uniform flow is assumed as an initial solution for the flow solver and a relaxation factor of 0.6 is used in the mesh movement algorithm. Specifically, the convergence history of both flow solver and adaptation grid procedures for the

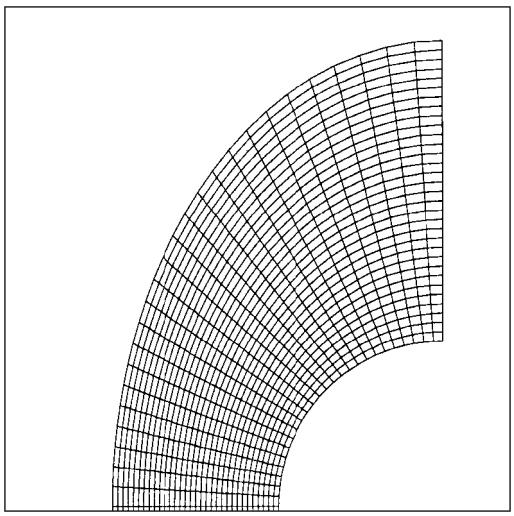

a) Initial grid

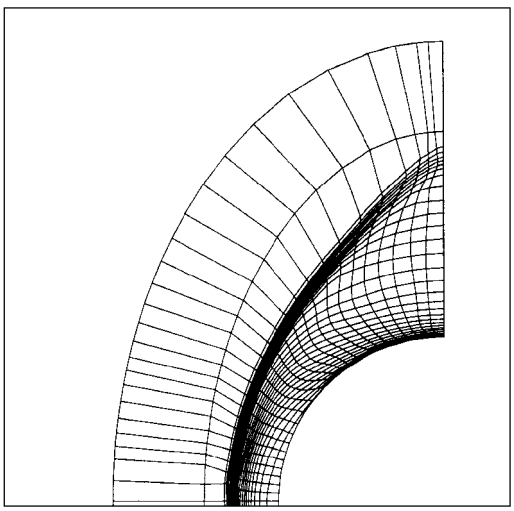

b) Final adapted grid

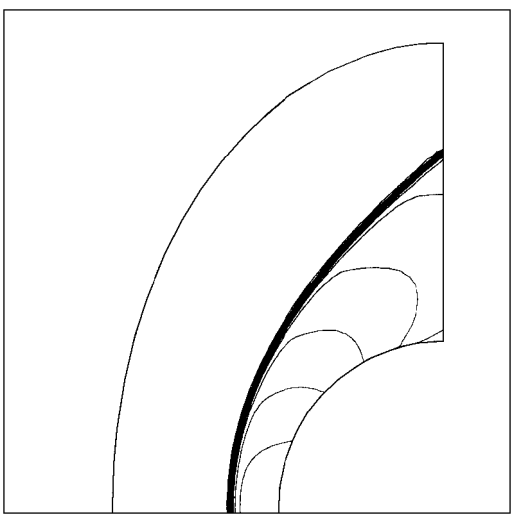

c) Final adapted solution in Mach number contours

Fig. 1 Mach 6.1 partially-dissociated nitrogen flow over a half-cylinder.

TCNE case are presented in Fig. 5, where the jumps in the curves represent the beginning of each new cycle. For a given value of the artificial dissipation coefficient, the L_2 norm of the solver's residual, at that cycle, is lowered by three orders of magnitude and then the mesh nodes are displaced 250 times.

Hypersonic Airflow over a Cylinder

In this example, the current methodology is applied to a hypersonic airflow over a half-cylinder with 50-mm radius. The free-

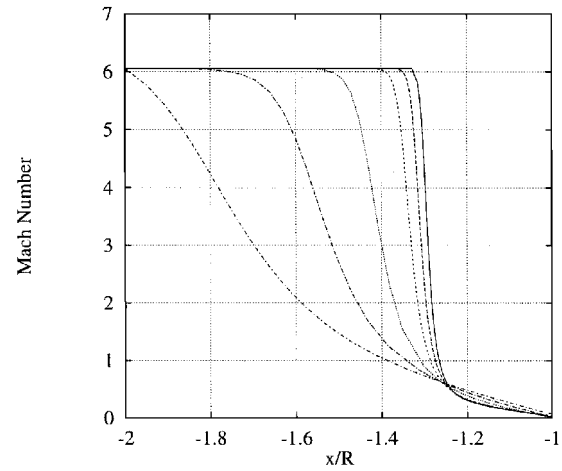

Fig. 2 Enhancement of the Mach number distribution, along the stagnation line, with grid adaptation cycles.

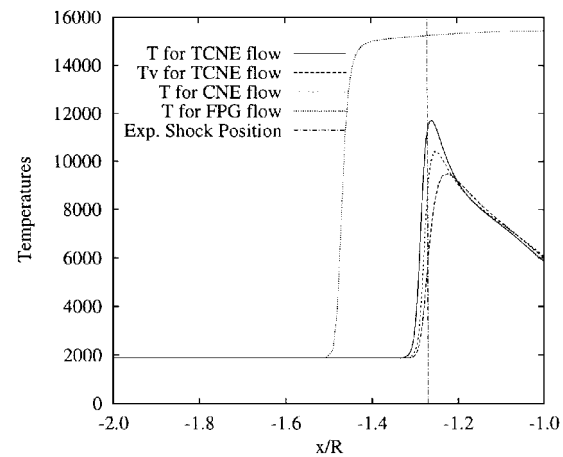

Fig. 3 Temperature distributions along the stagnation line.

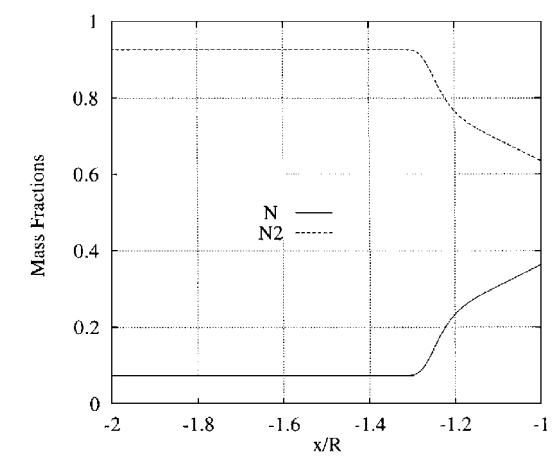

Fig. 4 Distributions of species mass fractions along the stagnation line.

stream conditions are $Ma_\infty = 12.7$, $T_\infty = 196$ K, and $\rho_\infty = 1.6 \times 10^{-3}$ kg/m^3. This test case was proposed in the Workshop on Hypersonic Flows for Reentry Problems (WHFRP),[22] and experimental results were obtained by Vetter et al.[23] for the same freestream conditions over a sphere.

The use of an adaptive procedure allows one to start the computation on the same grid as in the preceding test case (Fig. 1a), although the physics of the two flows are completely different. The final adapted grid and the corresponding temperature contours are shown in Fig. 6.

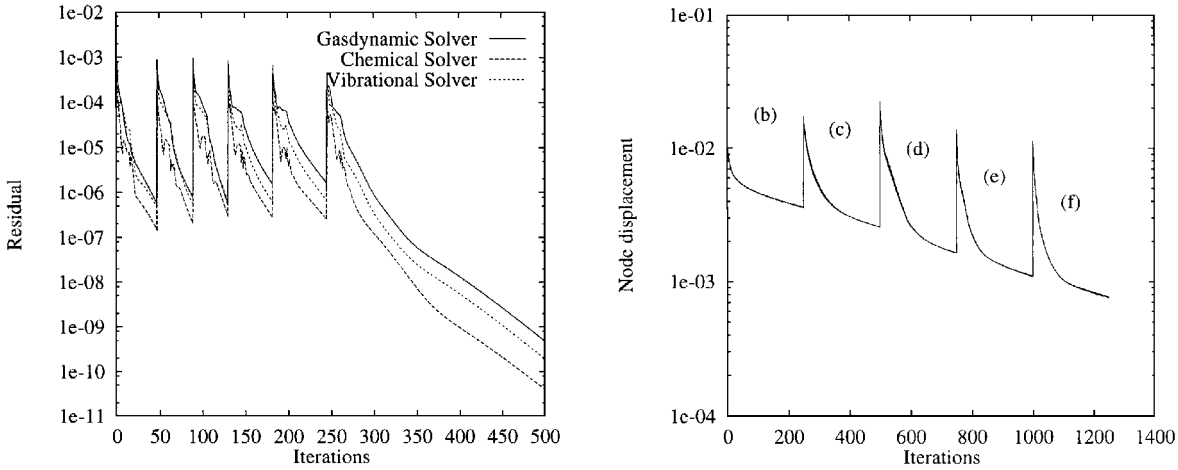

Fig. 5 Convergence histories of the flow solver and the adaptation procedure.

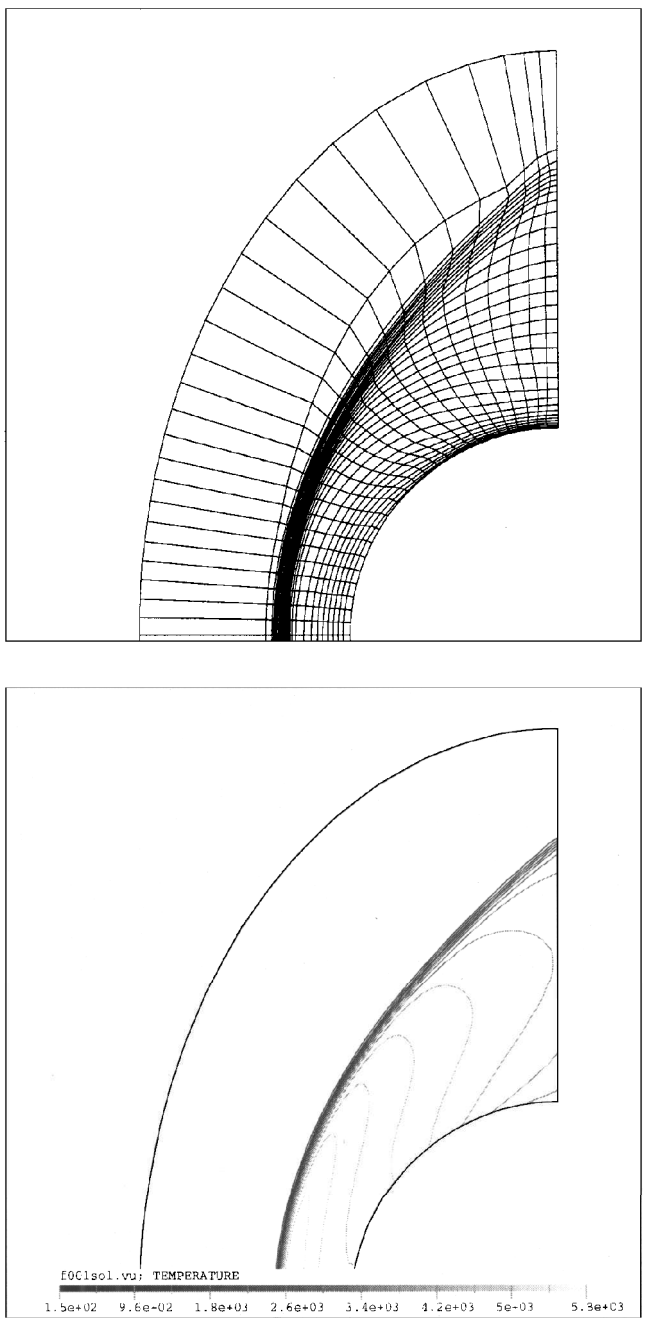

Fig. 6 Final adapted grid with the corresponding temperature contours.

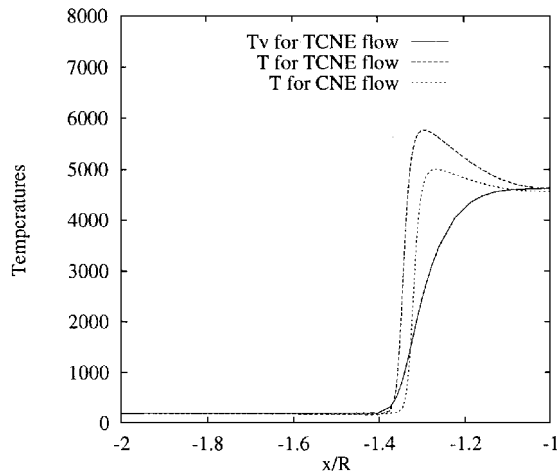

Fig. 7 Temperature distributions along the stagnation line.

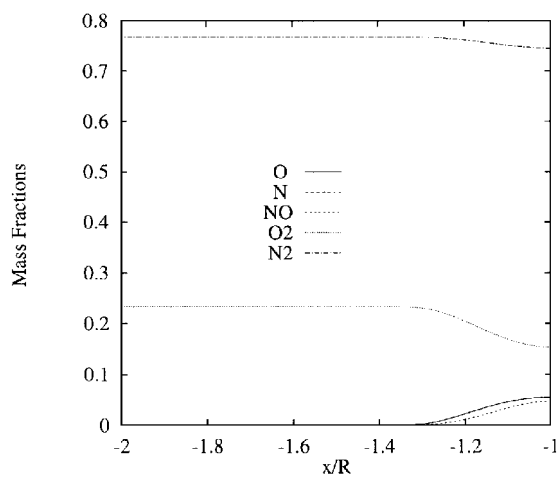

Fig. 8 Distributions of species mass fractions along the stagnation line.

The effect of the thermal state of the mixture on the translational temperature along the stagnation line is shown in Fig. 7. The same behavior of the thermochemical models as in the first benchmark can be observed with a peak in translational temperature of 5800 K in the TCNE case. Mass fraction plots of the five species are shown in Fig. 8, along the stagnation line. Nearly 40% of O_2 is dissociated, whereas the N_2 concentration remains almost constant.

The distribution of the pressure coefficient C_p on the cylinder in Fig. 9 shows a good agreement with the experiment. The superposition of C_p for TCNE, CNE, and FPG cases demonstrates its invariance with respect to reactions and vibrational relaxation phenomena.

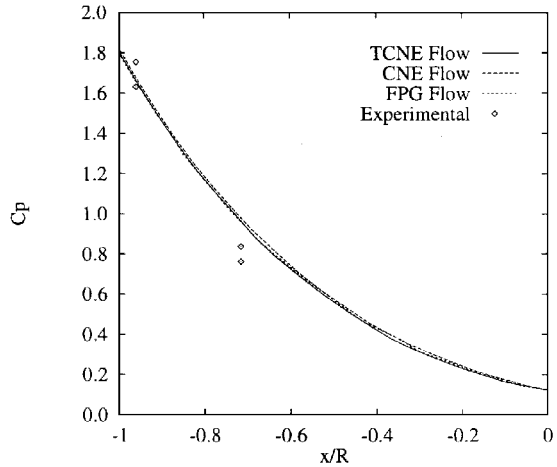

Fig. 9 Pressure coefficient distribution on the cylinder.

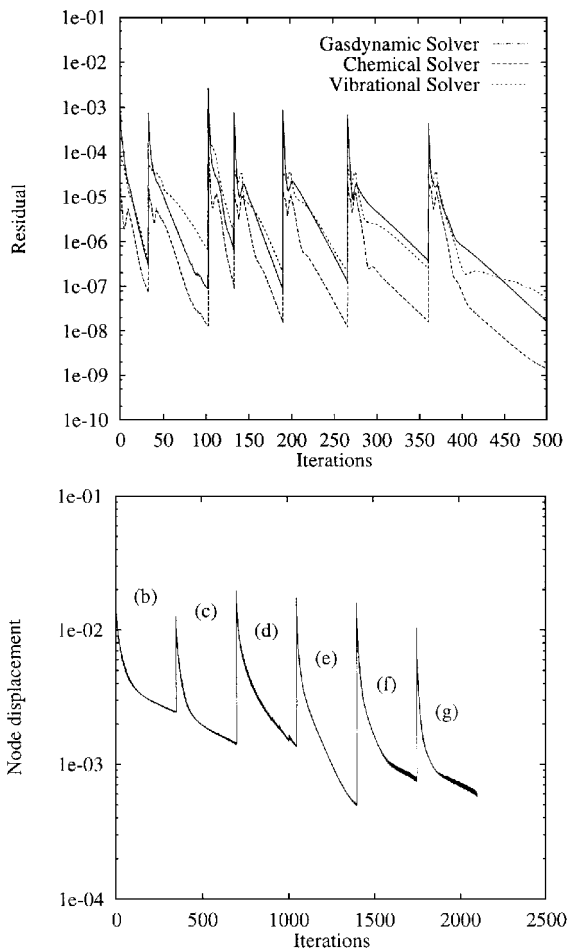

Fig. 10 Convergence histories of the flow solver and the adaptation procedure.

The steady-state solution is obtained by marching in time with different time steps for the gasdynamic, chemical, and vibrational systems. The solver's convergence displayed in Fig. 10 is obtained with the following chemical and vibrational time steps: $\Delta t^c = 0.4\,\Delta t^g$ and $\Delta t^v = 0.1\,\Delta t^g$. Here, Δt^g represents a local time step for the gasdynamic system and is computed according to a Courant–Friedrichs–Lewy number of 40. The convergence history of the adaptation procedure is also shown in Fig. 10, where a decrease of nearly two orders of magnitude in node displacement is achieved after six cycles of adaptation with 350 iterations per cycle.

Hypersonic Airflow over a Double Ellipse

In this test case, a double ellipse profile is placed into a Mach 12.7 flow at zero angle of attack. Since it was introduced in the WHFRP,[22] this benchmark has become an important challenge for

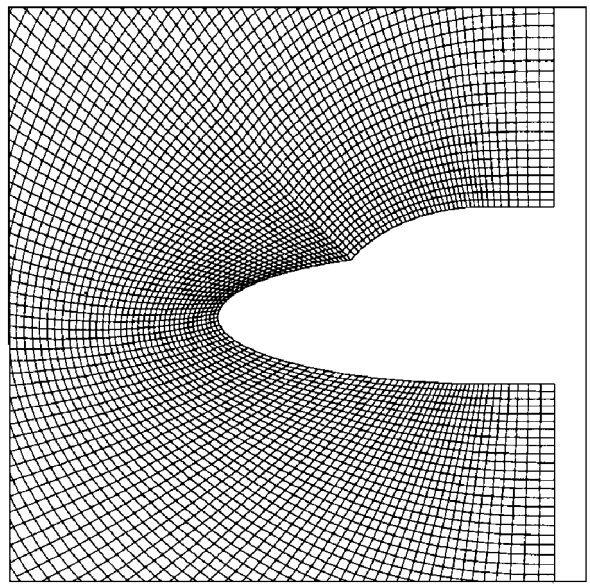

a) Initial grid

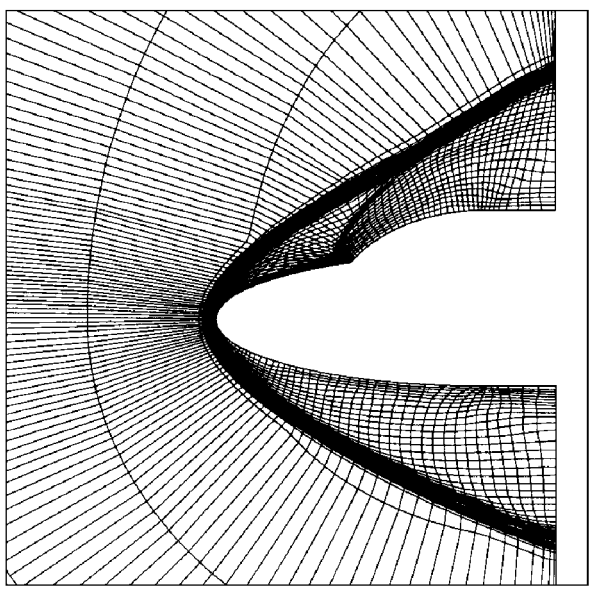

b) Final adapted grid

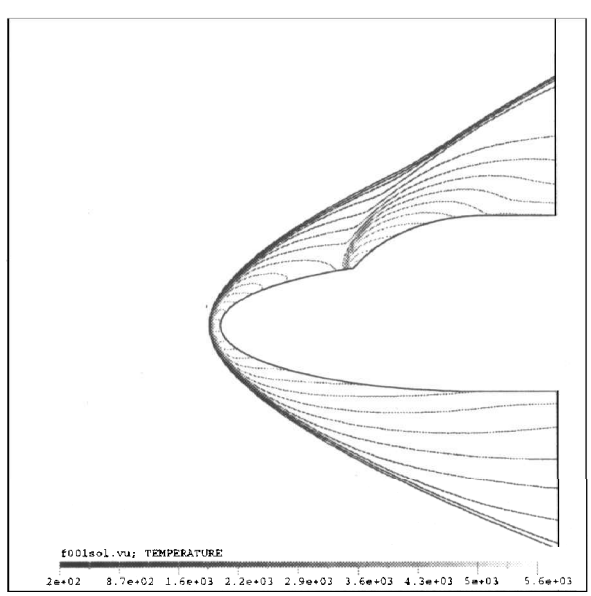

c) Final adapted solution in temperature contours

Fig. 11 Mach 12.7 thermochemical nonequilibrium airflow over a double ellipse.

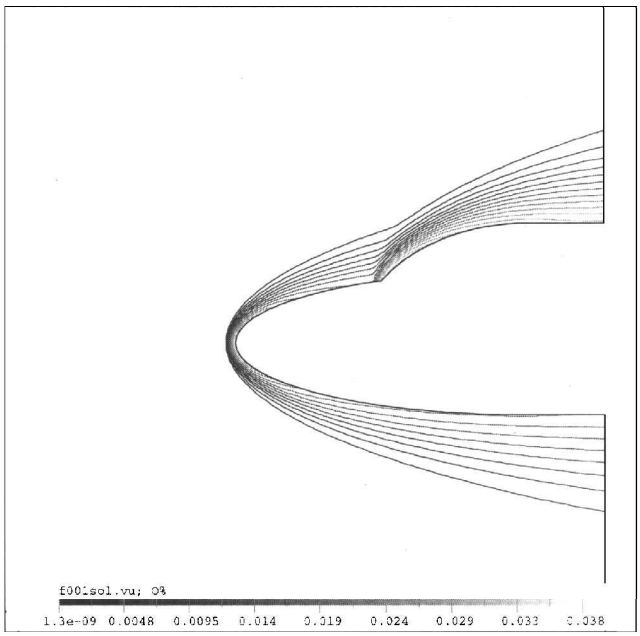

Fig. 12 Oxygen mass-fraction contours.

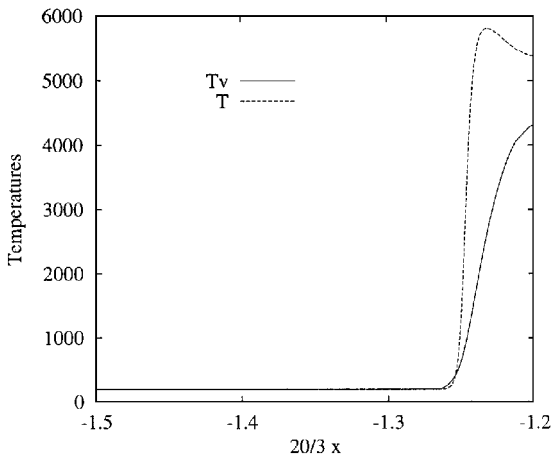

Fig. 13 Temperature distributions along the stagnation line.

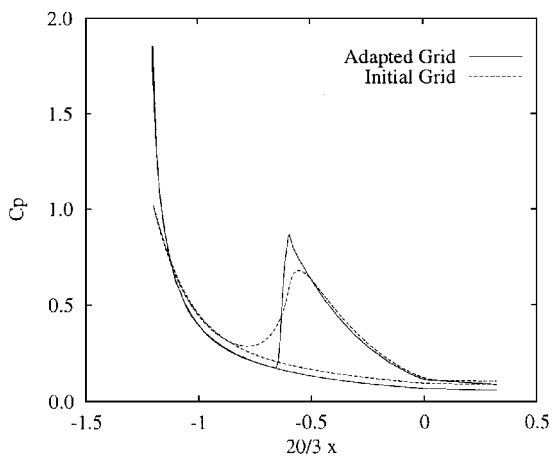

Fig. 14 Pressure coefficient on the body surface.

testing hypersonic flow solvers. The flowfield is characterized by a strong detached shock wave, followed by a moderate canopy shock and shock–shock interaction. Therefore, the application of mesh adaptation is highly suitable for efficiently resolving these different strength shocks.

The TCNE computation was initiated on a 45×124 (5580) grid that is shown in Fig. 11a. The adapted grid (Fig. 11b) is obtained after 6 levels of adaptation with 700 iterations each. The adapted solution is presented in Fig. 11c, and it can be seen that the detached and canopy shocks are well resolved.

The isocontours of monatomic oxygen concentration are shown in Fig. 12. The O_2 is only partially dissociated due the moderate temperatures of the flowfield. The distributions of the translational and vibrational temperatures along the stagnation line are presented in Fig. 13, revealing that the thermal equilibrium state is not reached at the stagnation point.

The pressure coefficient on the body surface is shown in Fig. 14 for the initial and final adapted grids. It can be clearly seen that the adapted mesh permits a much better capturing of the canopy shock, as well as of the flow properties at the stagnation point.

Conclusions

An implicit, finite element, segregated method has been described for two-dimensional, hypersonic, thermochemical nonequilibrium flows on directionally adapted grids. This loosely coupled approach has the advantage of reducing reacting flow problems, with a high number of species, to a manageable level and offers the possibility of applying the most appropriate numerical scheme to each system of PDE to achieve the best global convergence. The shocks have been efficiently resolved by coupling the flow solver to a mesh adaptation procedure. This adaptation method relies on an edge-based error estimate, as well as an improved mesh movement strategy with no orthogonality constraints, that is capable of achieving a wider nodal movement than current schemes. The resulting code is validated on hypersonic, partially dissociated, nitrogen flow where the shock position is correctly reproduced on a coarse mesh. The methodology is also tested for hypersonic airflows and the accurate prediction of the main flow features needed only coarse but adapted grids.

Acknowledgments

The authors would like to thank Natural Sciences and Engineering Research Council of Canada and Quebec's Fonds pour la Formation de Chercheurs et l'aide à la Recherche for their financial support of this work.

References

[1]Peraire, J., Vahdati, M., Morgan, K., and Zienkiewicz, O. C., "Adaptive Remeshing for Compressible Flow Computations," *Journal of Computational Physics*, Vol. 72, 1987, pp. 449–466.

[2]Fortin, M., Vallet, M.-G., Poirier, D., and Habashi, W. G., "Error Estimation and Directionally Adaptive Meshing," AIAA Paper 94-2221, June 1994.

[3]Ait-Ali-Yahia, D., Habashi, W. G., Tam, A., Vallet, M.-G., and Fortin, M., "A Directionally Adaptive Methodology Using an Edge-Based Error Estimate on Quadrilateral Grids," *International Journal for Numerical Methods in Fluids*, Vol. 23, 1996, pp. 673–690.

[4]Eberhardt, S., and Brown, K., "A Shock Capturing Technique for Hypersonic Chemically Relaxing Flows," AIAA Paper 86-0231, June 1986.

[5]Glaz, M. M., Colella, P., Collins, J. P., and Ferguson, R. E., "Nonequilibrium Effects in Oblique Shock-Wave Reflections," *AIAA Journal*, Vol. 26, No. 6, 1988, pp. 698–705.

[6]Liu, Y., and Vinokur, M., "Nonequilibrium Flow Computations. I. An Analysis of Numerical Formulations of Conservation Laws," *Journal of Computational Physics*, Vol. 83, 1989, pp. 373–397.

[7]Bussing, T. R. A., and Murman, E. M., "Finite Volume Method for the Calculation of Compressible Chemically Reacting Flows," AIAA Paper 85-0331, Jan. 1985.

[8]Park, C., and Yoon, S., "Fully Coupled Implicit Method for Thermo-Chemical Nonequilibrium Air at Suborbital Flight Speeds," *Journal of Spacecraft and Rockets*, Vol. 28, No. 1, 1991, pp. 31–39.

[9]Walters, R. W., Cinnella, P., Slack, D. C., and Halt, D., "Characteristic-Based Algorithms for Flows in Thermo-Chemical Nonequilibrium," *AIAA Journal*, Vol. 30, No. 5, 1992, pp. 1304–1313.

[10]Jonas, S., Fruhauf, H.-H., and Knab, O., "Fully Coupled Approach to the Calculation of Nonequilibrium Hypersonic Flows Using a Godunov-Type Method," *Computational Fluid Dynamics '92*, Vol. 1, Wiley, New York, 1992, pp. 305–314.

[11]Vincenti, W. G., and Kruger, C. H., *Introduction to Physical Gas Dynamics*, Krieger, Malabar, FL, 1986.

[12]Lee, J. H., "Basic Governing Equations for the Flight Regimes of Aeroassisted Orbital Transfer Vehicles," *Thermal Design of Aeroassisted Orbital Transfer Vehicles*, edited by H. F. Nelson, Vol. 96, Progress in Aeronautics and Astronautics, AIAA, New York, 1985, pp. 3–53.

[13]Millikan, R. C., and White, D. R., "Systematics of Vibrational Relaxation," *Journal of Chemical Physics*, Vol. 39, No. 12, 1963, pp. 3209–3213.

[14] Park, C., "Assessment of Two-Temperature Kinetic Model for Ionizing Air," *Journal of Thermophysics and Heat Transfer*, Vol. 3, No. 13, 1989, pp. 233–244.

[15] Park, C., "On Convergence of Computation of Chemically Reacting Flows," AIAA Paper 85-0247, Jan. 1985.

[16] Ait-Ali-Yahia, D., "A Finite Element Segregated Method for Hypersonic Thermo-Chemical Equilibrium and Nonequilibrium Flows Using Adapted Grids," Ph.D. Thesis, Dept. of Mechanical Engineering, Concordia Univ., Montreal, PQ, Canada, Nov. 1996.

[17] Gnoffo, A. P., "Hypersonic Flows over Biconics Using a Variable-Effective-Gamma Parabolized-Navier–Stokes Code," AIAA Paper 83-1666, 1983.

[18] Colella, P., and Glaz, P. M., "Efficient Solution Algorithms for the Riemann Problems for Real Gases," *Journal of Computational Physics*, Vol. 59, 1985, pp. 264–289.

[19] Nakahashi, K., and Deiwert, G. S., "Self-Adaptive Grid Method with Application to Airfoil Flow," *AIAA Journal*, Vol. 25, No. 4, 1987, pp. 513–520.

[20] Hornung, H. G., "Non-Equilibrium Dissociating Nitrogen Flow over Spheres and Cylinders," *Journal of Fluid Mechanics*, Vol. 53, No. 1, 1972, pp. 149–176.

[21] Candler, G. V., "On the Computation of Shock Shapes in Nonequilibrium Hypersonic Flows," AIAA Paper 89-0312, Jan. 1989.

[22] Abgrall, R., Désidéri, J.-A., Glowinski, R., Mallet, M., and Périaux, J. (eds.), *Hypersonic Flows for Reentry Problems*, Vol. 3, Springer–Verlag, New York, 1991.

[23] Vetter, M., Olivier, H., and Grönig, H., "Flow over Double Ellipsoid and Sphere–Experimental Results," *Hypersonic Flows for Reentry Problems*, Vol. 3, Springer–Verlag, New York, 1991, pp. 489–500.

J. Kallinderis
Associate Editor